Nano-Optomechanical Characterization and Manipulation of Photonic Crystals

Sushil Mujumdar, A. Femius Koenderink, Robert Wüest, and Vahid Sandoghdar

***Abstract*—We describe the application of scanning near-field optical microscopy (SNOM) for the high-resolution visualization of light propagation in photonic crystal structures. We also demonstrate that nanoscopic elements such as sharp tips could be used for the mechanical manipulation of the optical properties of photonic crystals. In particular, our theoretical and experimental results show that narrow resonances of a photonic crystal cavity can be tuned without a substantial influence on its quality factor. Furthermore, we discuss the modification of the fluorescence of a nanoscopic emitter as a function of its location close to a photonic crystal.**

***Index Terms*—Optical microelectromechanical systems (MEMS), photonic crystals, scanning near-field optical microscope, scanning near-field optical microscopy (SNOM), spontaneous emission.**

I. Introduction

THE SEARCH for highly compact miniaturized optical devices has acquired a constant momentum in the past years. A necessary feature that remains crucial to the effectiveness of such devices is the capability to manipulate the flow of light over short distances. Artificially created photonic bandgap crystals combined with other microstructures may provide an ideal platform to achieve control over the propagation of light in all three dimensions [1].

Photonic crystals consist of a periodic lattice of two dielectrics of dissimilar refractive indexes, with a lattice constant comparable to the wavelength of light in the crystal. The lattice planes act as Bragg reflectors that forbid the propagation of light for a range of frequencies and wave vectors. For suitable lattices with sufficiently high index contrast, a photonic bandgap may open, for which propagation is forbidden for all wave vectors.

Although 3-D photonic bandgap crystals have been reported, their fabrication remains quite challenging. As a result, most of the recent activities have focused on the realization of 2-D membrane structures where light confinement in the third dimension is achieved by total internal reflection [2]–[4]. A common 2-D crystal consists of a lattice of air holes, electrochemically etched or lithographically drilled into a semiconductor wafer and then subjected to postprocessing to yield an ultrathin membrane. The large refractive index contrast between the semiconductor and air creates a wide bandgap for the TE-guided mode of the membrane, and ensures an efficient confinement of light in the transverse direction via total internal reflection.

Several functional optical devices have been developed based on the membrane photonic crystal platform, including ultrahigh-Q cavities and low-loss waveguides [2], [3]. When heterogeneities are introduced in a photonic crystal environment, modes may be created for certain frequencies inside the bandgap, and light can be bound to the site of the inhomogeneity. For instance, if a defect is engineered in a lattice of holes by filling one of them with a dopant material, a microresonator can be obtained. If a complete row of holes is filled, a linear waveguide is created. By using permutations and combinations of line and point defects, one can obtain more complex functionalities such as sharply bent waveguides, Y-splitters, add-and-drop filters, and so on [5]–[10]. Thus, photonic crystal-based elements are promising versatile building blocks in optical nanodevices. In this paper, we will discuss some possibilities for punctual, dynamic and reversible modification, and modulation of photonic crystals by mechanical manipulation at the subwavelength level.

As microelectromechanical systems (MEMS) and optical MEMS develop in sophistication, we could think of exploiting their capabilities for manipulating the flow of light in photonic crystals in a controllable and reversible fashion at the nanometer scale. A first essential step toward controlling the flow of light in this fashion is to map out and understand the features of the light-field distribution inside the microstructure. Conventional imaging techniques rely on the out-of-plane scattering of light, which is expected to be minimal in the case of a high-quality 2-D PC. Moreover, in a PC structure, the electromagnetic-field distribution strongly varies over a subwavelength scale and is, thus, inaccessible to far-field imaging because of the Rayleigh criterion. Here, scanning near-field optical microscopy (SNOM) can be applied to visualize the confinement and propagation of light with a very high resolution [11]–[13]. In this method, a sharp optical probe is brought into close proximity of the sample to tap into the evanescent fields over the surface. Since these fields are nonpropagating, the resolution does not depend upon the Rayleigh criterion, but is only limited by the probe diameter and its separation from the surface. An optical resolution of 100 nm is routinely achieved in SNOM. An added benefit of this technique is that one can measure the topography of the sample concurrently with the optical data. SNOM has been applied to the study of light propagation and confinement in photonic crystals by a number of groups [14]–[24].

Manuscript received October 12, 2006; revised October 12, 2006.

S. Mujumdar was with the Laboratory of Physical Chemistry, ETH Zurich, 8093 Zurich, Switzerland. He is now with the Tata Institute of Fundamental Research, Mumbai 400005, Maharashtra, India (e-mail: mujumdar@tifr.res.in).

A. F. Koenderink was with the Laboratory of Physical Chemistry, ETH Zurich, 8093 Zurich, Switzerland. He is now with the Center for Nanophotonics, FOM Institute for Atomic and Molecular Physics, 1098 SJ Amsterdam, The Netherlands (e-mail: f.koenderink@amolf.nl).

R. Wüest and V. Sandoghdar are with the Laboratory of Physical Chemistry, ETH Zurich, 8093 Zurich, Switzerland (e-mail: robert.wueest@phys.chem.ethz.ch; vahid.sandoghdar@ethz.ch).

Digital Object Identifier 10.1109/JSTQE.2007.893744

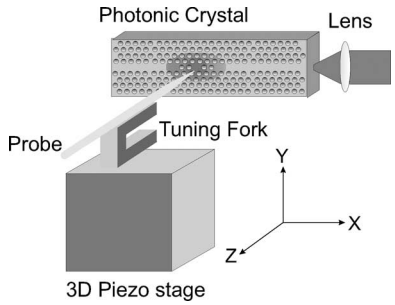

Fig. 1. Schematic of the SNOM setup for measuring the light flow. The laser light is focussed onto the incoupling waveguide, while the SNOM probe scans the near-field evanescent light in the region of interest. The probe is attached to a quartz tuning fork, that is installed on a 3-D piezoelectric translation stage. The SNOM fiber tip directs the collected light to an APD.

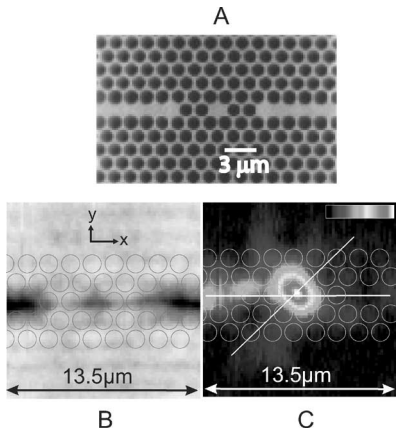

Fig. 2. (a) SEM image of a photonic crystal point-defect microcavity. The point defect as well as the incoupling and outcoupling waveguides are illustrated. (b) Topography image as measured by a low-resolution SNOM. The point defect and the waveguides are discernible enough to enable reconstruction of the photonic crystal structure. (c) Optical data as provided by the SNOM probe. The measured light-field distribution shows that its axes of symmetry are tilted with respect to the longitudinal axis. This information reveals the departure of the underlying PC resonator from the ideal structure [19], [26].

In this paper, we will describe our theoretical and experimental efforts toward achieving optomechanical functionality in photonic crystal devices. We first describe the SNOM technique in detail, and demonstrate its capability in mapping the flow of light in PC microresonators and waveguides. We then report our theoretical studies of external tuning of the resonant frequency in the particular case of a microresonator. We go on to validate these predictions by our experimental results on the frequency tuning of a high-Q microcavity. Finally, we show that one can also control the excited state lifetimes of emitters placed at the extremities of sharp tips by varying the relative position between the emitters and the photonic crystal environment.

II. Near-Field Optical Imaging of Photonic Crystals

The central idea in SNOM is to interrogate high spatial frequency evanescent fields of a sample. The most elementary example of a sample is the diffraction grating with a subwavelength period. Although the zeroth order of this grating cannot propagate, evanescent fields on its surface follow the periodicity of the grating. Thus, a local subwavelength detector, in an ideal case a single atom, could read out the field and intensity distribution. Because the high spatial frequency near fields decay rapidly away from the surface, it is imperative that SNOM measurements are performed in the immediate vicinity of the surface. To ensure a subwavelength size and the ability to follow tiny features of a surface at close proximity, sharp tips are used. The resolution obtained by SNOM is, thus, determined by the size of the tip and its separation from the sample. An account of the basic principles of operation of SNOM and its applications for imaging photonic devices can be found in [13].

An SNOM measurement setup is depicted in Fig. 1, and consists of a fiber tip that is glued onto a quartz tuning fork. The tuning fork is mounted onto a piezo-controlled translation stage that allows 3-D movement. A tip-surface distance of ~ 10 nm is maintained with the help of the quartz tuning fork using shear-force feedback [25]. In this method of feedback, the tuning fork and, hence, the tip are made to oscillate with a motion parallel to the surface. When the tip-sample distance is reduced to ~ 10 nm, a frictional force between the surface and the tip acts to damp its oscillation, changing its phase and amplitude. Control of the amplitude or the phase in a servo loop allows to hold the tip at a fixed distance from the surface. By recording the control signal of the shear-force control during a lateral scan, one can retrieve the topographical map of the sample. Concurrently, radiation scattered by the tip is partially collected by the fiber itself, which, in our case, is connected to an InGaAs avalanche photodiode (APD) photon counting module. In this way, the topography and the optical signal of the device are recorded simultaneously.

We demonstrate the application of SNOM by giving two examples, i.e., a point defect resonator and a line defect waveguide. In both devices, the aim was to study the exact electromagnetic field distribution relative to the defect sites and as a function of the wavelength.

Fig. 2 displays the SNOM observations of a resonator region of a PC sample. A line-defect waveguide was fabricated in a macroporous silicon photonic crystal. Two pairs of holes separated by a point defect were etched in the line defect. The central point defect functioned as a cavity, while the neighboring line defects worked as the incoupling and outcoupling waveguides, as shown in Fig. 2(a). Fabricated for mid-infrared wavelengths, the structure had two resonances at 3.62 and 3.84 μm. To allow detection in this wavelength region, fluoride glass tips were employed. The fluoride tips are very fragile and prone to breakage. For this reason, the probe in this run was not very sharp, leading to a low lateral topography resolution. We note that while a sharp tip is highly desirable for high-quality topography maps in the visible wavelength regime, a duller tip provides a larger signal. Fig. 2(c) shows the intensity distribution, when the laser wavelength was tuned to the resonance at $\lambda = 3.84$ μm. The propagation of light in the first waveguide and its confinement about the point defect are clearly seen. These particular data revealed several unexpected features, which, with the aid of careful numerical simulations, could be traced to very slight deviations of the structure parameters from the ideal design [19], [26].

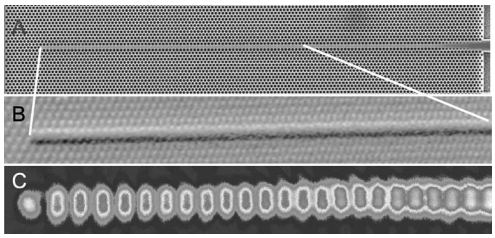

Fig. 3. Terminated waveguide to serve as a standing wave meter. (a) SEM image of a tapering waveguide. (b) Topography map of the waveguide as detected by a high-resolution SNOM tip. (c) Optical intensity map of the light in the waveguide, showing a standing wave [24].

This indicates that SNOM can be a powerful tool to assess the fabrication accuracy of microdevices.

With recent progress in the fabrication of high-quality PC structures in the near infrared, SNOM measurements have also been applied to the investigation of light propagation in these structures [21], [27]. In Fig. 3, we present studies on a structure that consists of a slab waveguide with a core of InGaAsP (400 nm, $n = 3.45$) and an upper InP cladding layer (200 nm, $n = 3.18$). The vertical slab waveguide supports one TE mode with an effective index of $n_{\text{eff}} = 3.29$ at $\lambda = 1550$ nm. The PC structure uses a triangular array of holes (depth $\approx 3\,\mu$m) with a lattice constant of $a = 430$ nm. This results in a photonic bandgap for TE light for a range of reduced frequencies of $u = a/\lambda = 0.27 - 0.43$. Further details on the sample and its fabrication can be found elsewhere [28], [29]. Fig. 3(c) shows SNOM measurement at $\lambda = 1490$ nm of a waveguide that was terminated at one end. The SEM image, the topography, and the simultaneously recorded intensity distribution are illustrated in the figure. These data enabled us to analyze stationary wave patterns in the waveguide for a range of frequencies, and to determine the waveguide dispersion and loss with a high accuracy [24]. We point out that SNOM has also been used to reveal a rich temporal behavior in photonic samples, using heterodyne time-resolved measurement techniques [23], [30].

III. Manipulation of the Device Functionality Using Nanoscopic Elements

Having shown that SNOM can image photonic devices at the subwavelength scale, one might wonder whether the tip affects the light flow. Several years ago, we showed that a glass fiber tip could even image the light flow in whispering gallery microresonators of very high quality factor [32] without perturbing it. However, we also showed that a tip could lower the Q and introduce frequency shifts if it is thick enough [31]. In principle, this lesson could also be extended to photonic crystals, but because the mode volume in the latter is usually much smaller, the effect of the tip is stronger. In order to quantify this, we have performed finite-difference time domain (FDTD) calculations [33], [34]. We have found that for certain tip parameters, it is possible to shift the resonance frequency of a PC microresonator without affecting its Q in a substantial manner. We also found that the presence of the tip can introduce resonances in a PC without any defects.

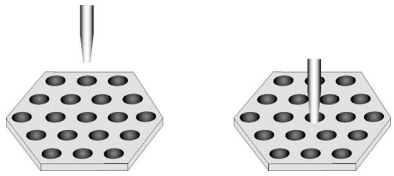

Fig. 4. Schematic illustration of an optomechanical switch, realized by inserting a sharp probe into one hole of a hexagonal lattice of a PC membrane.

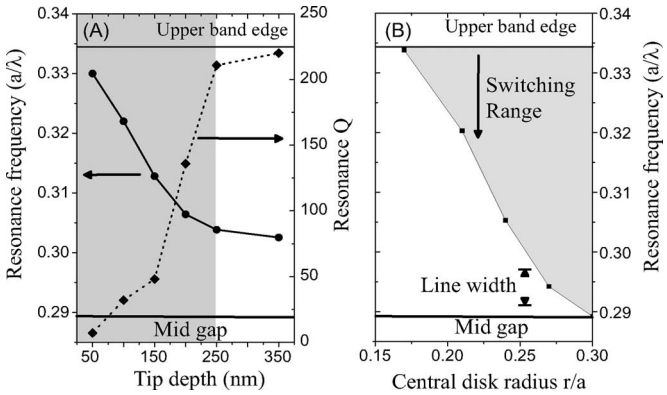

Fig. 5. Creation of a low-Q resonance by inserting a silicon tip into one hole of a defect-free photonic crystal. (a) Calculated resonance frequency (circles, solid line, left-hand axis) and the Q factor (diamonds, dotted line, right-hand axis) as a function of the tip depth in the hole. The gray shaded area indicates the membrane width. (b) Dependence of the resonance frequency on tip radius for fully inserted tips. The gray shaded area is the available switching range. The arrow couplet shows the line width associated with this resonance that can be created on demand.

A. On Command Creation of Resonances in Photonic Crystals

As a case study, we first report on the realization of an optomechanical switch, wherein a low-Q microcavity resonance is switched on using a near-field probe. The system under study is an ultrathin membrane made of silicon onto which a 2-D PC with a hexagonal lattice is etched. We assumed a slab dielectric constant $\epsilon = 11.76$ typical for silicon, a membrane thickness of 250 nm, lattice constant $a = 420$ nm, and a hole radius $r = 0.3a$. Crystals over $5\,\mu\text{m} \times 5\,\mu\text{m}$ in lateral size surrounded by up to $1\,\mu$m of air were simulated, applying Liao's absorbing boundary conditions. We used computational meshes with 14 or 20 grid points per a parallel to the membrane, with twice the resolution normal to the membrane [35]. Grid cell volume averaging of the dielectric constant was employed to reduce staircasing errors [36]. Q factors and cavity mode frequencies were obtained by fitting a damped harmonic wave to time traces of the total E-field energy in the cavity. The probes were assumed to be cylindrical in shape, and were assigned several values of the dielectric constant to simulate different materials ranging from glass to silicon.

Let us consider the effect of such a probe inserted into a hole of the defect-free PC membrane, as illustrated in Fig. 4. The presence of the probe causes a point-defect in the lattice. As shown in Fig. 5(a), introducing a silicon tip $(\epsilon = 11.76)$ with a diameter of 200 nm into a hole in a photonic crystal membrane indeed pulls down a resonance from the top of the gap. The frequency shows a linear decrease with the tip's progression

further into the membrane, but saturates once the tip protrudes all the way through the membrane. At this point, the Q factor of the resonance reaches its maximum of ~ 250. In Fig. 5(b), we see that the maximum tuning range is determined by the diameter of the tip. The maximum tuning range of half the gap width (as much as 150 nm) is obtained for a tip that completely fills an air hole [37]. In practice, however, it is desirable to use thinner tips. Because the resonance Q factor is limited to only about 250, there is a minimum practical tip radius for which the shift of the resonance away from the upper band edge exceeds its linewidth. Such a situation is achieved for the tip radii above $0.2a$. High index tips, such as silicon AFM tips are required for this type of switching because tips from materials such as glass fail to provide the necessary index contrast for creating resonances well separated from the band edge.

The aforementioned arrangement provides an optomechanical switching or filtering functionality with a Q of ~ 200. Since there is no direct contact or physical interaction between the probe and the membrane, this mode is as temporary as the presence of the probe in the proximity of the membrane. Furthermore, since the interaction of the tip with the electromagnetic mode of the PC is via the evanescent fields, the tip functionality has a spatial range of only about a few tens of nanometers. Thus, the actuation can be extremely fast.

B. Nanomechanical Tuning of Resonances in Photonic Crystal Microresonators

An important functionality in photonic circuits is the ability to tune the frequency of a device continuously, in a reproducible and reversible manner. Along the same lines as the optomechanical switch, we also studied a tuning method where an external probe is brought into the vicinity of a resonator to shift its frequency in a continuous and reversible manner. We describe the results of our 3-D FDTD simulations, where a point-defect resonator is perturbed by a cylindrical dielectric tip.

In this simulation, the photonic crystal membrane was identical to that of the previous case, except that a resonator was created using the design proposed in [4]. Initially, a point defect of reduced radius $r = 0.15a$ is created in the PC. Next, by reducing the radius of two holes to $r = 0.23a$ on either side of the defect and shifting them outwards by $0.11a$, a nondegenerate dipole mode is created. The intensity profile of this mode is shown in Fig. 6. This resonant mode lies in the center of the 2-D TE bandgap, and has a frequency $\omega a/2\pi c = 0.284$ with a Q around 13 000. Thus, for telecom wavelengths of $\lambda = 1500$ nm, the resonance linewidth turns out to be 15 GHz. The Q factor of such a mode is low enough to be simulated by 3-D time-domain calculations without any difficulties. Yet, Q is high enough for useful tuning effects to be demonstrated. In addition, this type of cavity mode has a large amplitude in the central air-hole, which is accessible to a near-field probe.

As seen in Fig. 7, a significant frequency shift occurs when a silicon tip is approached to the center of the cavity. If the tip is more than a few tens of nanometers away from the PC membrane, the loss is insignificant. In this regime, the frequency shift increases exponentially as the tip is approached. Up to shifts of

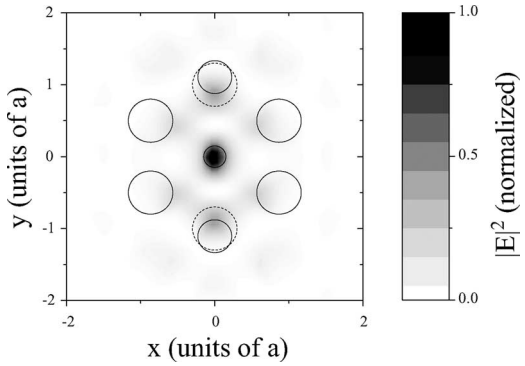

Fig. 6. Design of the high-Q cavity consisting of a central defect in a hexagonal lattice. The defect radius is $0.15a$. The lattice constant for this membrane is 420 nm, hole radius $0.3a$, and the dielectric constant is 11.76. Two holes neighboring the defect are shifted and shrunk in order to optimize the cavity. The intensity map shows the electric field intensity $|E|^2$ of the resonant mode, as calculated from 3-D FDTD.

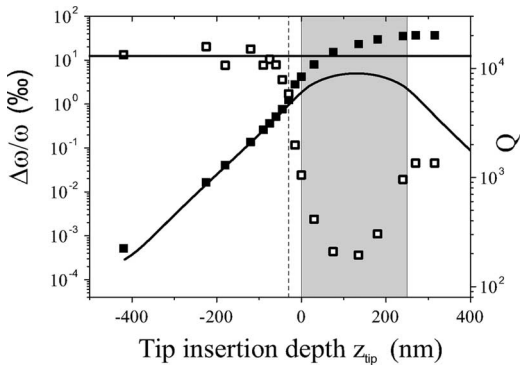

Fig. 7. Relative induced frequency shift (solid symbols, left-hand axis) and the Q-factors (open symbols, right-hand axis) as a function of the tip depth calculated for the cavity in Fig. 6. The tip is 125 nm in diameter and centered above the central defect hole. The gray area denotes the membrane. Negative depth indicates that the tip apex is still away from the surface. The frequency shift follows the mode profile $|E|^2$ (solid curve). The loss is minimal for tips up to 30 nm away from the membrane (vertical dashes). The horizontal line shows the Q-factor in the absence of the tip.

around 250 GHz, equivalent to 2 nm at a wavelength of 1500 nm and an order of magnitude larger than the cavity linewidth, low losses with Q above 5000 can be maintained. Evidently, the detuning increases exponentially as the tip penetrates deeper into the evanescent field over the PC membrane. When the tip approaches closer to the membrane, say, for tip-membrane separations below 20 nm, the cavity Q factor drops below 5000, down to about 200 for a tip inserted into the central defect hole. For tips not fully inserted into the central defect, field profiles show strong scattering normal to the membrane on the side away from the tuning probe. However, once the probe fully extends through the slab, the quality factor recovers to about 1000.

To obtain a physical understanding of the variation of the tuning and the loss in the presence of a perturbation, we have applied an exact theory originally developed for perturbations in microwave cavities [33], [38]. We find that the frequency shift is essentially limited by the ratio of the effective tip polarizability to the cavity mode volume V_{cav}. The effective polarizability of

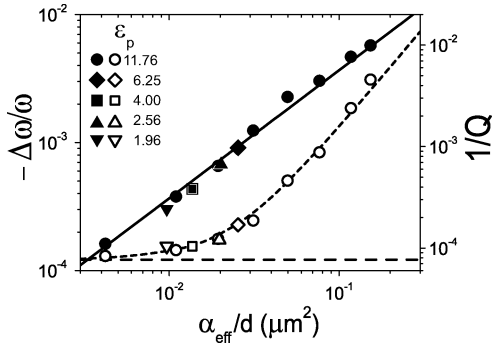

Fig. 8. Relative frequency shift (solid symbols, left-hand axis) and $1/Q$ (open symbols, right-hand axis) *versus* the effective polarizability per length $\alpha_{\rm eff}/d = 3(\epsilon_{\rm p}-1)/(\epsilon_{\rm p}+2)\pi r_{\rm p}^2$. The tip is positioned 30 nm above the central defect in Fig. 6. Various tip materials (Si, TiO_2, ZrO_2, polystyrene, and SiO_2) were simulated as indicated in the legend. The frequency shift is proportional to $\alpha_{\rm eff}$ (solid curve). The horizontal dashed line is the loss $1/Q$ in the absence of the tip. This loss when added to a contribution proportional to $\alpha_{\rm eff}^2$ gives the total loss, as shown by the dashed curve.

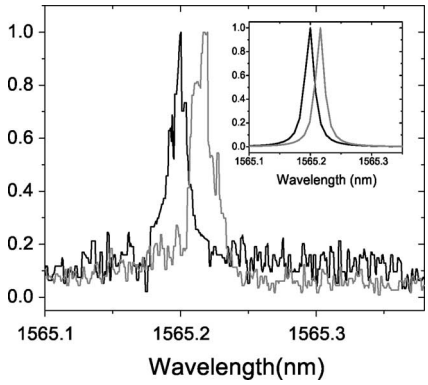

Fig. 9. Experimentally measured frequency shift in the presence of a SNOM tip in the proximity of a PC microcavity. The resonance of the perturbed PC is red-shifted due to a weak interaction with the silica tip. The inset shows Lorentzian fits to the experimental spectra.

the tip is given by [38], [39]

$$\alpha = 3\frac{\epsilon-1}{\epsilon+2}V_{\rm tip}, \quad \text{with} \quad V_{\rm tip} = \pi r_{\rm tip}^2 d$$

where the tip volume corresponds to the tip cross section $\pi r_{\rm tip}^2$ times an effective height d set by the exponential decay length of the mode into which the tip is inserted. It turns out that the frequency shift increases linearly with the volume of the perturber, while the loss contribution only grows quadratically with the tip polarizability. This behavior provides a regime, wherein one can achieve good tunability without incurring undesirable losses. It turns out that the relative frequency shift as a function of the tip's lateral coordinate $\mathbf{r}_\parallel$ and its height $z_{\rm tip}$ above the sample can be approximated by

$$\frac{\Delta\omega(\mathbf{r}_\parallel, z_{\rm tip})}{\omega} = -\frac{\alpha_{\rm eff}}{2V_{\rm cav}}\frac{|E_0(\mathbf{r}_\parallel)|^2}{\max[\epsilon(\mathbf{r})|E_0|^2]}e^{-z_{\rm tip}/d}. \quad (1)$$

As the tip is scanned over the surface at a constant height, the obtained frequency shift is a direct map of the electric field intensity profile $|E_0|^2$ for the cavity mode just above the slab (shown in Fig. 6). Thus, a large tuning of the magnitude of the frequency shift can be modulated either by retracting the tip upwards, or moving the tip sideways over distances on the order of 50 nm away from the central cavity hole. We emphasize that the scheme discussed here is quite general, and is applicable to any other cavity design as long as the tip and cavity parameters are chosen properly.

Fig. 8 shows that the tuning effect predicted by FDTD for silicon tips scales linearly with the tip polarizability and, hence, with the tip cross section $\pi r_{\rm tip}^2$, while the loss induced by the tip scales quadratically with the tip polarizability. Such quadratic dependence is consistent with an interpretation of loss as Rayleigh scattering off the tip. We have carried out extensive simulations, wherein different cavity designs and different tip refractive indexes were used to obtain the tuning, and we have confirmed that the induced frequency shift is set by the ratio of polarizability to cavity mode volume. We also show that the quadratic scaling of loss with α allows to maintain a reasonably high Q above 5000 at a large frequency shift of 260 GHz [33].

We performed experimental studies on high-Q photonic crystal microcavities to validate our proposal of optomechanical control of microcavity resonance frequencies [40]. The PC microcavities were etched in a GaAs membrane, using a double heterostructure layout [41], [42]. Resonances with Q factors of the order of 10^4 were obtained. An uncoated sharp tip of silica ($\epsilon = 1.96$) was brought into the near field of the resonator region. The incident laser frequency was swept through a range encompassing the PC resonant frequency, where the tip recorded a strong optical signal. The resonant frequency was measured both for the tip in the near field and when it was retracted into the far field. In the latter case, the tip could still pick up a fraction of the light scattered out of the resonator by the surface inhomogeneities. The observations are shown in Fig. 9. The right-hand spectrum was recorded for the tip in the near field, and the left-hand spectrum was obtained for the unperturbed resonator. The inset of the figure shows the Lorentzian best-fit profiles for the two data sets. Evidently, there is no significant effect on the Q of the resonance, but there is a clear frequency shift of about $\Delta\omega/\omega = -1.2\times10^{-4}$. The details of these studies are to be published elsewhere [40].

We note that even though loss and frequency scale intuitively with the magnitude of the perturbation, there is no obvious relation between the frequency shift and the induced loss that holds for all tip positions. For instance, our calculations show tip positions for which a large loss is induced, without an appreciable frequency shift. A detailed analysis shows that the induced loss strongly depends on the polarization of the mode at the position of the tip. For tip positions where the electric field has a large contribution normal to the membrane and along the tip, light is scattered strongly into the tip [43].

Fig. 10 illustrates these phenomena for the single-hole cavity that we consider in Fig. 6. At position I, right above the central hole, a large frequency shift of 260 GHz is obtained by a silicon tip of 125-nm diameter at a tip height of 30 nm. Concomitantly, the presence of the tip lowers the Q from 13 000 to just above 5000. In agreement with the very low mode intensity at position

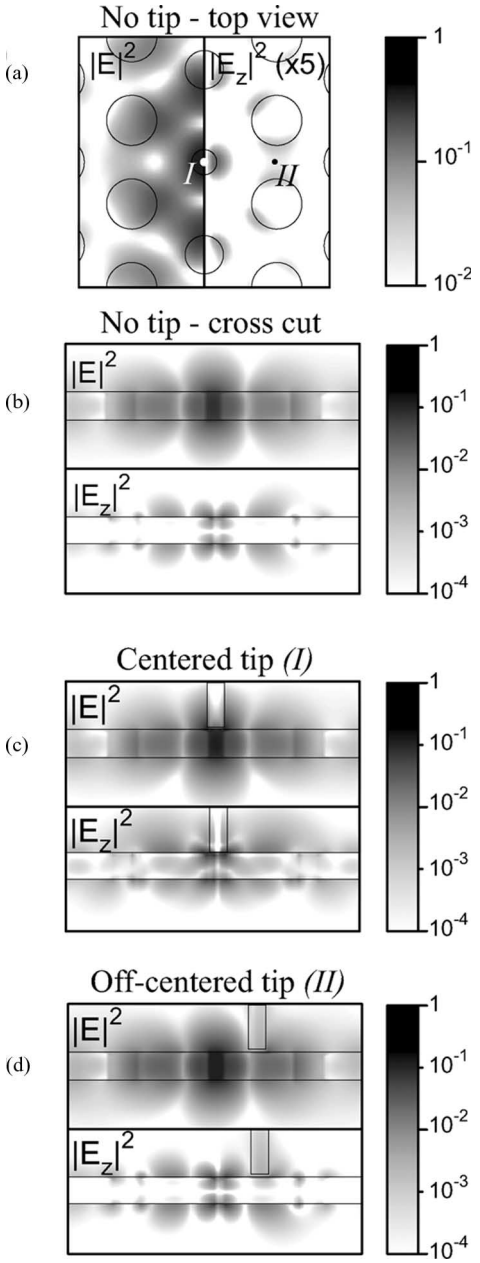

Fig. 10. Electric field intensity profiles (logarithmic grayscales) for the cavity in Fig. 6. (a) and (b) Tip absent. (c) Silicon tip situated 30 nm above the membrane, above the central hole (position I). (d) Silicon tip situated 30 nm above the membrane, laterally displaced from the central hole (position II). The left panel in (a) corresponds to the cycle-averaged $|E|^2$ summed over all vector components, while the right panel in (a) corresponds to the component $|E_z|^2$ normal to the membrane only (scaled by a factor 5 for visibility). Likewise, in panels (b)–(d), the top (bottom) represents the total field (normal component of the field). Circles in (a) indicate the outlines of the air holes. Horizontal lines in (b)–(d) indicate the top and bottom of the 250-nm-thick membrane. The tip outline is also indicated in (c) and (d). Panel (a) corresponds to the fields in a plane parallel to and just 15 nm above the membrane. Panels (b)–(d) are crosscuts normal to the membrane through the line from position I to II. In (d), there is a significant leakage into the tip.

II, the frequency shift induced by the same tip at position II is less than 15 GHz, i.e., less than the linewidth of the unperturbed cavity. Despite the small frequency shift, the drop in Q at position II is comparable to that at position I, due to the fact that position II is right above a lobe with a strong electric field normal to the slab [Fig. 10(a), right half, and (b)]. Indeed, cross sections of the field intensity in Fig. 10(b)–(d) show that the field is scattered into the tip especially strongly at position II. In contrast, for tip position I, the electric field is expelled away from the tip.

In summary, there are tip positions where the induced frequency shift is vanishingly small, in accordance with the low overall density of the mode at the tip position, but where significant loss is induced due to the polarization selectivity of the near-field probe. It has been shown that the loss of photonic crystal microcavities can be dramatically reduced by minute changes in the near-field mode profile that strongly affect the far-field interference [2], [4]. In this light, it may even be possible to reduce losses of cavities by a suitable placement of a nanoscopic perturbation.

C. Mechanical Control of Fluorescence via Coupling to Photonic Crystals

In this section, we examine the possibility of modifying and controlling the fluorescence of emitters by nanomechanical motion. It has been known for several decades that the spontaneous emission rate of an atom as well as its radiation pattern can be modified if it is placed in a resonator [44], or close to a surface [45] or nanostructure [46]. This phenomenon is usually explained by the fact that the density of states available for the emission of the atom at a certain position is modified, when boundary conditions are considered for the electromagnetic field. In fact, the possibility for a strong modification of the spontaneous emission was one of the original driving forces for the invention and investigation of photonic crystals [47]. It turns out that in all geometries, the fluorescence rate and angular spread depend very sensitively on the exact position of the emitter at the subwavelength scale. In the case of PC structures, the most commonly considered scenario concerns an emitter embedded in a PC [48]. Given the strong sensitivity of the optical field and the density of states to displacements of only a few tens of nanometers, the great difficulty is then to optimize the effect for a given emitter. Recently, a clever technique has been developed to address this issue during the fabrication process [49]. Here, we discuss a scheme where the emitter is coupled to 2-D PCs externally via the evanescent fields, so that its position can be adjusted at will. Our strategy is to mount a single emitter or a nanoscopic ensemble of emitters to the end of a subwavelength object such as a tip [50]–[53]. Besides the possibility of optimizing the lateral position of the emitter, this approach has a great advantage that the coupling strength could be actuated in real time from zero to its maximum value.

We have studied the effect of the PC bandgap on the excited state lifetime of the active material, with particular emphasis on its lateral position relative to the crystal lattice. In this study, we employed the 3-D FDTD method [54]–[56] to calculate the local radiative density of states (LRDOS), accounting for the position dependence of the photon states available for the fluorescent decay of a quantum emitter [57]. This calculation relies on the fact that the LRDOS appearing in the formulation of Fermi's

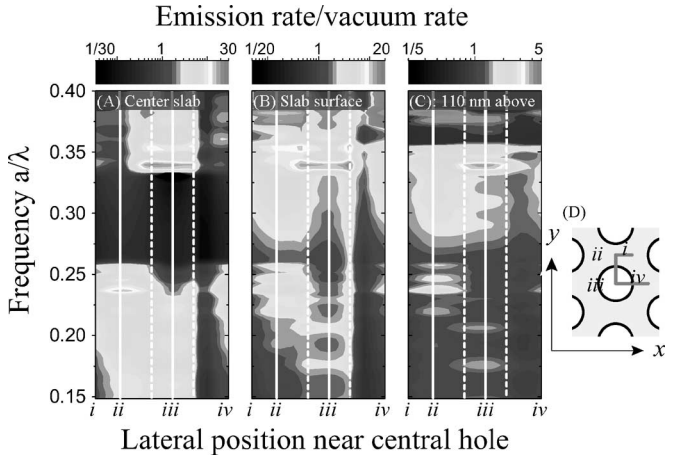

Fig. 11. Emission rate/vacuum rate for an x-oriented dipole as a function of frequency and position along the trajectory indicated by the gray line in (d). (a) In middepth. (b) On the surface. (c) 110 nm above the PC membrane. (d) Trajectory tracing the edges of the irreducible part of the unit cell. The dashed lines in (a)–(c) mark the borders between air and dielectric [58].

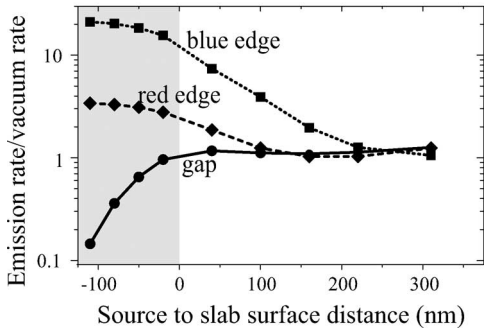

Fig. 12. Emission rate modification as a function of the height of a dipole above the PC membrane. Circles, diamonds, and squares show data for $a/\lambda = 0.23, 0.28, 0.34$, corresponding to frequencies below, in, and above the gap, respectively. The shaded region shows the range of positions $-125 < z < 0$ nm in the membrane.

Golden Rule for spontaneous emission rate, also describes the total emitted power of a classical point dipole antenna run at a fixed current [54]. The PC samples simulated were membranes with dielectric constant $\epsilon = 11.76$ and thickness $d = 250$ nm, surrounded by up to $1\,\mu$m of air above and below. We took the membrane to contain a hexagonal array of holes with radius $r = 0.3a$ at a lattice spacing of $a = 420$ nm. We used discretization with 14 or 20 points per lattice constant, and employed volume-averaging of the dielectric constant to reduce staircasing errors [33]. We considered finite hexagonally shaped PC structures up to 25 holes across, terminated by the unperforated slab extending into Liao's absorbing boundary conditions. By broadband temporal excitation of the dipole, we simulated the emission power spectrum over a wide frequency range. The results that we present correspond to the LRDOS normalized to that in vacuum [56].

Fig. 11 displays the modification of the LRDOS for the dipole when positioned: 1) in the middepth of the membrane; 2) right at the crystal–air interface; and 3) at 110 nm above this plane. These data reveal that as z increases, the inhibition and enhancement reduce in size. To examine this distance dependence more closely, in Fig. 12, we plot the normalized emission rate as a function of the distance between the dipole and the membrane surface for three key frequencies $a/\lambda = 0.23, 0.28$, and 0.34 just below, in, and just above the bandgap, respectively. Evidently, the inhibition diminishes for emitters located above the slab. In contrast, enhancements persist at the blue edge of the gap even if the dipole is lifted into air above the membrane. Thus, it appears that it is possible to enhance the spontaneous emission rate by a factor of 5–10, if the emitter position is controlled to within 50 nm above the PC membrane. Note that the emission of a dipole near a simple homogeneous dielectric slab is also enhanced, due to coupling to the guided modes. However, at the gap edges, the PC causes a further strong enhancement of the LRDOS [58], [59].

Fig. 11(a) also shows a contour plot of the LRDOS modification for an x-oriented dipole midway in the slab depth *versus* emission frequency and for lateral locations along a trajectory that traces the irreducible part of the unit cell [Fig. 11(d)]. The emission is inhibited in the bandgap at all positions, whereas outside the gap, we observe Fabry–Pérot modulations, together with enhancement at the low- and high-frequency edges. The enhancement of the emission occurs especially on the high frequency edge of the gap (the "air band") for dipoles in air holes and, predominantly, at the low-frequency edge (the "dielectric band") for dipoles in the dielectric.

The aforementioned calculations show that nanomechanical manipulation of an emitter close to a surface can modulate its fluorescence rate. Furthermore, the efficiency of the coupling between an emitter and a photonic crystal, and its radiation pattern can be controlled by the actuation of small displacements in the lateral or axial directions. The modification of the emission is expected to be even more sensitive to distance variations, if the PC structure contains resonances.

IV. Conclusion

In this paper, we have reviewed how SNOM can be a great asset for the characterization of the light flow in photonic crystals. Furthermore, we have shown that the strong spatial modulation of light fields in these structures opens interesting avenues for influencing their functionalities. We have presented a few such ideas for on-command switching and tuning of passive devices, and have discussed the possibility of controlling the coupling of an emitter to photonic crystal devices. Our approach has been to exploit nanoscopic mechanical elements that can be actuated at will at the surface of a photonic crystal. We predict that cavities, waveguide bends, interferometers, directional couplers, and filters can be tuned using this method in a compact and flexible fashion.

Acknowledgment

The samples described in Section II were fabricated in FIRST, the Center for Micro- and Nanoscale Science at ETH Zurich. The samples in the experiments of frequency tuning were fabricated at the Nanodevices for Photonics and Electronics Group at the University of Würzburg. The authors thank U. Gösele

and coworkers at the Max-Planck-Institut in Halle, as well as R. Wehrspohn at the University of Paderborn for a fruitful collaboration on macroporous silicon photonic crystals, and D. Erni, P. Strasser, F. Robin, and H. Jäckel at the Photonic Communication Group of ETH Zurich for InP-based photonic crystals. They are also grateful to M. Kafesaki, IESL-FORTH, Crete, and C. M. Soukoulis, IESL-FORTH, Crete and Iowa State University, for their support in numerical calculation, and to B. Buchler for stimulating discussions. This work was carried out in the framework of the Network of Excellence ePIXnet and the priority program SP 1113 of the Deutsche Forschungsgemeinschaft (DFG).

REFERENCES

[1] C. M. Soukoulis, Ed., *Photonic Crystals and Light Localization in the 21st Century*, Dordrecht, The Netherlands: Kluwer, 2001.

[2] Y. Akahane, T. Asano, B. S. Song, and S. Noda, "High-Q photonic nanocavity in a two-dimensional photonic crystal," *Nature*, vol. 425, pp. 944–947, 2003.

[3] S. J. McNab, N. Moll, and Y. A. Vlasov, "Ultra-low loss photonic integrated circuit with membrance-type photonic crystal waveguides," *Opt. Express*, vol. 11, pp. 2927–2939, 2003.

[4] J. Vučković, M. Lončar, H. Mabuchi, and A. Scherer, "Design of photonic crystal microcavities for cavity QED," *Phys. Rev. E*, vol. 65, p. 016608-01, 2001.

[5] A. Chutinan and S. Noda, "Waveguides and waveguide bends in two-dimensional photonic crystal slabs," *Phys. Rev. B*, vol. 62, pp. 4488–4492, 2000.

[6] A. Mekis, J. C. Chen, I. Kurland, S. Fan, P. R. Villeneuve, and J. D. Joannapoulos, "High transmission through sharp bends in photonic crystal waveguides," *Phys. Rev. Lett.*, vol. 77, pp. 3787–3790, 1996.

[7] M. Tokushima and H. Yamada, "Light propagation in a photonic-crystal-slab line-defect waveguide," *IEEE J. Quantum Electron.*, vol. 38, no. 7, pp. 753–759, Jul. 2002.

[8] S. Y. Lin, E. Chow, J. Bur, S. G. Johnson, and J. D. Joannapoulos, "Low-loss, wide-angle Y splitter at approximately $\sim 1.6 - \mu$m wavelengths built with a two-dimensional photonic crystal," *Opt. Lett.*, vol. 27, pp. 1400–1402, 2002.

[9] S. Noda, A. Chutinan, and M. Imada, "Trapping and emission of photons by a single defect in a photonic bandgap structure," *Nature (London)*, vol. 407, pp. 608–610, 2000.

[10] A. Chutinan, M. Mochizuki, M. Imada, and S. Noda,, "Surface-emitting channel drop filters using single defects in two-dimensional photonic crystal slabs," *Appl. Phys. Lett.*, vol. 79, pp. 2690–2692, 2001.

[11] D. W. Pohl, W. Denk, and M. Lanz, "Optical stethoscopy: Image recording with resolution lambda/20," *Appl. Phys. Lett.*, vol. 44, pp. 651–653, 1984.

[12] A. Lewis, M. Isaacson, A. Harootunian, and A. Muray, "Development of a 500 Å spatial resolution light microscope: I. light is efficiently transmitted through $\cdot/16$ diameter apertures," *Ultramicroscopy*, vol. 13, pp. 227–231, 1984.

[13] V. Sandoghdar, B. C. Buchler, P. Kramper, S. Götzinger, O. Benson, and M. Kafesaki, "Scanning nearfield optical studies of photonic devices," in *Photonic Crystals.Advances in Design, Fabrication, and Characterization*, K. Busch, S. Lölkes, R. Wehrspohn, and H. Föll, Eds. Weinheim, Germany: Wiley-VCH, 2004, pp. 215–237.

[14] P. Kramper, A. Birner, M. Agio, C. M. Soukoulis, F. Müller, U. Gösele, J. Mlynek, and V. Sandoghdar, "Direct spectroscopy of a deep two-dimensional photonic crystal microresonator," *Phys. Rev. B*, vol. 64, p. 233102-01, 2001.

[15] S. I. Bozhevolnyi, V. S. Volkov, J. Arentoft, A. Boltasseva, T. Søndergaard, and M. Kristensen, "Direct mapping of light propagation in photonic crystal waveguides," *Opt. Commun.*, vol. 212, pp. 51–55, 2002.

[16] S. I. Bozhevolnyi, V. S. Volkov, T. Søndergaard, A. Boltasseva, P. I. Borel, and M. Kristensen, "Nearfield imaging of light propagation in photonic crystal waveguides: Explicit role of Bloch harmonics," *Phys. Rev. B*, vol. 66, p. 235204-01, 2002.

[17] D. Gerard, L. Berguiga, F. de Fornel, L. Salomon, C. Seassal, X. Letartre, P. Rojo-Romeo, and P. Viktorovitch, "Near-field probing of active photonic-crystal structures," *Opt. Lett.*, vol. 27, pp. 173–175, 2002.

[18] D.-J. Shin, S.-H. Kim, J.-K. Hwang, H.-Y. Ryu. H.-G. Park, D.-S. Song, and Y.-H. Lee, "Far- and near-field investigations on the lasing modes in two-dimensional photonic crystal slab lasers," *IEEE J. Quantum Electron.*, vol. 38, no. 7, pp. 857–866, Jul. 2002.

[19] P. Kramper, M. Kafesaki, C. M. Soukoulis, A. Birner, F. Müller, R. Wehrspohn, U. Gösele, J. Mlynek, and V. Sandoghdar, "Near-field visualization of light confinement in a photonic crystal microresonator," *Opt. Lett.*, vol. 29, pp. 174–176, 2004.

[20] E. Flück, M. Hammer, W. L. Vos, N. F. van Hulst, and L. Kuipers, "Near-field probing of photonic crystals," *Photon. Nanostruct.*, vol. 2, pp. 127–135, 2004.

[21] K. Okamoto, M. Loncar, T. Yoshie, A. Scherer, Y. M. Qiu, and P. Gogna *Appl. Phys. Lett.*, vol. 82, pp. 1676–1678, 2003.

[22] H. Gersen, T. J. Karle, R. J. P. Engelen, W. Bogaerts, J. P. Korterik, N. F. van Hulst, T. F. Krauss, and L. Kuipers, "Real-space observation of ultraslow light in photonic crystal waveguides," *Phys. Rev. Lett.*, vol. 94, p. 073903-01, 2005.

[23] H. Gersen, T. J. Karle, R. J. P. Engelen, W. Bogaerts, J. P. Korterik, N. F. van Hulst, T. F. Krauss, and L. Kuipers, "Direct observation of Bloch harmonics and negative phase velocity in photonic crystal waveguides," *Phys. Rev. Lett.*, vol. 94, p. 123901-01, 2005.

[24] R. Wüest, D. Erni, P. Strasser, F. Robin, H. Jäckel, B. C. Buchler, A. F. Koenderink, V. Sandoghdar, and R. Harbers, "A "standing-wave meter" to measure dispersion and loss of photonic-crystal waveguides," *Appl. Phys. Lett.*, vol. 87, p. 261110-01, 2005.

[25] K. Karrai and R. D. Grober, "Piezoelectric tip-sample distance control for near field optical microscopes," *Appl. Phys. Lett.*, vol. 66, p. 1842, 1995.

[26] B. C. Buchler, P. Kramper, M. Kafesaki, C. M. Soukoulis, and V. Sandoghdar, "Near-field optical investigations of photonic crystal microresonators," *IEICE Trans. Electron.*, vol. E87-C, pp. 371–377, 2004.

[27] N. Louvion, D. Gerard, J. Mouette, F. de Fornel, C. Seassal, X. Letartre, A. Rahmani, and S. Callard, "Local observation and spectroscopy of optical modes in an active photonic-crystal microcavity," *Phys. Rev. Lett.*, vol. 94, p. 113907-01, 2005.

[28] P. Strasser, R. Wüest, F. Robin, K. Rauscher, B. Wild, D. Erni, and H. Jäckel, "An ICP-RIE etching process for InP-based photonic crystals using $Cl/_2$//Ar/N/$_2$/ chemistry," in *Proc. 17th Int. Conf. Indium Phosphide Related Mater.*, Glassgow, U.K., May 8–12, 2005, pp. 242–245.

[29] R. Wüest, B. C. Buchler, R. Harbers, P. Strasser, K. Rauscher, F. Robin, D. Erni, V. Sandoghdar, and H. Jäckel,, "Near-field optical microscopy of light propagation through photonic crystal waveguide tapers," *Proc. SPIE*, vol. 5840, 2005, pp. 110–117.

[30] M. L. M. Balistreri, H. Gersen, J. P. Korterik, L. Kuipers, and N. F. van Hulst, "Tracking femtosecond laser pulses in space and time," *Science*, vol. 294, pp. 1080–1082, 2001.

[31] S. Götzinger, O. Benson, and V. Sandoghdar, "Towards controlled coupling between a high-Q whispering gallery mode and a single nanoparticle," *Appl. Phys. B*, vol. 73, pp. 825–828, 2001.

[32] S. Götzinger, O. Benson, and V. Sandoghdar, "Influence of a sharp fiber tip on high-Q modes of a microsphere resonator," *Opt. Lett.*, vol. 27, pp. 80–82, 2002.

[33] A. F. Koenderink, M. Kafesaki, B. C. Buchler, and V. Sandoghdar, "Controlling the resonance of a photonic crystal microcavity by a near-field probe," *Phys. Rev. Lett.*, vol. 95, p. 153904-01, 2005.

[34] A. F. Koenderink, R. Wüest, B. C. Buchler, S. Richter, P. Strasser, M. Kafesaki, A. Rogach, R. B. Wehrspohn, C. M. Soukoulis, D. Erni, F. Robin, H. Jäckel, and V. Sandoghdar, "Near field optics and control of photonic crystals," *Photon. Nanostruct.*, vol. 3, pp. 63–74, 2005.

[35] M. Kafesaki, M. Agio, and C. M. Soukoulis, "Waveguides in finite-height two-dimensional photonic crystals," *J. Opt. Soc. Am. B*, vol. 19, pp. 2232–2240, 2002.

[36] O. Hess, C. Hermann, and A. Klaedtke, "Finite-Difference time-domain simulations of photonic crystal defect structures," *Phys. Status Solidi A*, vol. 197, pp. 605–619, 2003.

[37] P. R. Villeneuve, S. Fan, and J. D. Joannopoulos, "Microcavities in photonic crystals: Mode symmetry, tunability, and coupling efficiency," *Phys. Rev. B*, vol. 54, pp. 7837–7842, 1996.

[38] R. A. Waldron, "Perturbation theory of resonant cavities," *Proc. Inst. Elect. Eng.*, vol. 107C, pp. 272–274, 1960.

[39] J. D. Jackson, *Classical Electrodynamics*. New York: Wiley, 1975.

[40] S. Mujumdar *et al.* , submitted for publication.

[41] B.-S. Song, S. Noda, T. Asano, and Y. Akahane, "Ultra-high-Q photonic double-heterostructure nanocavity," *Nat. Mater.*, vol. 4, pp. 207–210, 2005.

[42] R. Herrmann, T. Sünner, T. Hein, A. Löffler, M. Kamp, and A. Forchel, "Ultrahigh-quality photonic crystal cavity in GaAs," *Opt. Lett.*, vol. 31, pp. 1229–1231, 2006.

[43] C. Girard, A. Dereux, O. J. F. Martin, and M. Devel, "Importance of confined fields in near-field optical imaging of subwavelength objects," *Phys. Rev. B*, vol. 50, p. 14467-01, 1994.
[44] E. M. Purcell, "Spontaneous emission probabilities at radio frequencies," *Phys. Rev.*, vol. 69, pp. 681–681, 1946.
[45] K. H. Drexhage, "Interaction of light with monomolecular dye layers," in *Progress in Optics*vol. 12, E. Wolf, Ed. North Holland: Amsterdam, The Netherlands, 1974, pp. 163–232.
[46] C. Henkel and V. Sandoghdar, *Opt. Commun.*, vol. 158, pp. 250–262, 1998.
[47] E. Yablonovitch, "Inhibited spontaneous emission in solid-state physics and electronics," *Phys. Rev. Lett.*, vol. 58, pp. 2059–2062, 1987.
[48] A. Badolato, K. Hennessy, M. Atatüre, J. Dreiser, P. M. Petroff, and A. Imamoglu, "Deterministic coupling of single quantum dots to single nanocavity modes," *Science*, vol. 308, pp. 1158–1161, 2005.
[49] K. Hennessy, A. Badolato, A. Tamboli, M. Petroff, E. Hu, M. Atatüre, J. Dreiser, and A. Imamoglu, "Tuning photonic crystal nanocavity modes by wet chemical digital etching," *Appl. Phys. Lett.*, vol. 87, p. 0211080-01, 2005.
[50] T. Kalkbrenner, U. Hakanson, A. Schädle, S. Burger, C. Henkel, and V. Sandoghdar, "Optical microscopy via spectral modifications of a nanoantenna," *Phys. Rev. Lett.*, vol. 95, p. 200801-01, 2005.
[51] S. Kühn, C. Hettich, C. Schmitt, J. P. H. Poizat, and V. Sandoghdar, "Diamond colour centres as a nanoscopic light source for scanning near-field optical microscopy," *J. Microsci.*, vol. 202, pp. 2–6, 2001.
[52] J. Michaelis, C. Hettich, J. Mlynek, and V. Sandoghdar, "Optical microscopy using a single-molecule light source," *Nature*, vol. 405, pp. 325–328, 2000.
[53] V. Zwiller, T. Aichele, F. Hatami, W. T. Masselink, and O. Benson, "Growth of single quantum dots on preprocessed structures: Single photon emitters on a tip," *Appl. Phys. Lett.*, vol. 86, p. 091911-01, 2005.
[54] R. K. Lee, Y. Xu, and A. Yariv, "Modified spontaneous emission from a two-dimensional photonic bandgap crystal slab," *J. Opt. Soc. Am. B*, vol. 17, pp. 1438–1442, 2000.
[55] A. Taflove and S. C. Hagness, *Computational Electrodynamics: The Finite-Difference Time-Domain Method*, 2nd ed. Boston, MA: Artech House, 2000.
[56] C. Hermann and O. Hess, "Modified spontaneous emission rate in an inverted-opal structure with complete photonic bandgap," *J. Opt. Soc. Am. B*, vol. 19, pp. 3013–3018, 2002.
[57] R. Sprik, B. A. van Tiggelen, and A. Lagendijk, "Optical emission in periodic dielectrics," *Europhys. Lett.*, vol. 35, pp. 265–270, 1996.
[58] A. F. Koenderink, M. Kafesaki, C. M. Soukoulis, and V. Sandoghdar, "Spontaneous emission in the near-field of 2D photonic crystals," *Opt. Lett.*, vol. 30, pp. 3210–3212, 2005.
[59] A. F. Koenderink, M. Kafesaki, C. M. Soukoulis, and V. Sandoghdar, "Spontaneous emission rates of dipoles in photonic crystal membranes," *J. Opt. Soc. Am. B*, vol. 23, pp. 1196–1206, 2006.

Sushil Mujumdar received the Ph.D. degree from Raman Research Institute, Bangalore, Karnataka, India.

He was a Postdoctoral Researcher in the European Laboratory for Nonlinear Spectroscopy (LENS), Florence, Italy, followed by the University of Alberta, Edmonton, Canada, and then at the Swiss Federal Institute of Technology Zurich, Zurich, Switzerland. He is currently setting up his own research program in nanooptics at the Tata Institute of Fundamental Research, Mumbai, India. His research interests include several aspects of light propagation in disordered media including random lasers, biomedical imaging, and near-field studies of photonic crystals.

A. Femius Koenderink received two M.Sc. degrees in physics and in applied mathematics from Utrecht University, Utrecht, The Netherlands, in 1998 and 1999, respectively. He received the Ph.D. degree from the University of Amsterdam, Amsterdam, The Netherlands, in 2003.

From 2003 to 2005, he was a Postdoctoral Researcher at the Swiss Federal Institute of Technology Zurich, Zurich, Switzerland. He then joined the Center for Nanophotonics at the FOM Institute for Atomic and Molecular Physics, Amsterdam. His current research interests include nanooptics in carefully engineered subwavelength structures of resonant nanoparticles.

Robert Wüest received the M.Sc. degree in physics from the University of Basel, Basel, Switzerland, in 2000, and the Ph.D. degree from the Electronics Laboratory, Swiss Federal Institute of Technology (ETH) Zurich, Zurich, Switzerland.

He was an R&D Engineer with Optospeed, Zurich. He is currently a Postdoctoral Researcher in the Nano-Optics Group, ETH Zurich. His research interests include fabrication and optical characterization of nanophotonic devices.

Vahid Sandoghdar was born in Tehran, Iran. He received the B.S. degree in physics from the University of California, Davis, and the Ph.D. degree in atomic physics from Yale University, New Haven, CT.

He carried on research at the Ecole Normale Superieure, Paris, France, before moving to Konstanz, Germany, where he obtained the habilitation in physics. Since 2001, he has been the Chair in nanooptics at the Swiss Federal Institute of Technology Zurich, Zurich, Switzerland.